Supplementary Materials

Influence of Synthesis-Related Microstructural Features on the Electrocaloric effect for 0.9Pb(Mg$_{1/3}$Nb$_{2/3}$)O$_3$–0.1PbTiO$_3$ ceramics

Hana Uršič [1,2,*,+], **Marko Vrabelj** [1,2,+], **Mojca Otoničar** [1,2], **Lovro Fulanović** [1,2,3], **Brigita Rožič** [1,2], **Zdravko Kutnjak** [1,2], **Vid**

A. Literature review

**Table S1.** Comparison of the EC properties for PMN-PT ceramics prepared by columbite and mechanochemical syntheses.

Composition	Synthesis method	T (°C)	ΔT_{EC} (°C)	E (kV/cm)	d (μm)	Ref.
PMN	Col	69	1.42	90	100–130	[1]
PMN-5PT	Col	68	1.14	50	100–130	[1]
PMN-8PT	Col	30	0.58	20	1000	[2]
PMN-10PT	Col	89	1.19	50	100–130	[1]
PMN-13PT	SS*	70	0.56	24	1000	[3]
PMN-15PT	Col	124	1.28	50	100–130	[1]
PMN-20PT	Col	141	1.41	50	100–130	[1]
PMN-25PT	Col	110	0.9¥	25	1000	[4]
PMN-25PT	Col	146	1.30	50	100–130	[1]
PMN-30PT	Col	183	1.53	50	100–130	[1]
PMN	Mech	67	2.56	90	60–100	[5]
PMN-10PT+	Mech	107	2.77	160	80	[6]
PMN-10PT++	Mech	127	3.45	160	80	[6]
PMN-30PT	Mech	157	2.70	90	60–100	[5]

Mech – mechanochemical synthesis, Col – columbite synthesis, SS* – solid-state synthesis/direct reactive sintering method, ¥Calculated from the Q data, c$_P$ values were taken from [7], +ceramics with GS of 2.8 μm, ++ceramics with GS of 3.6 μm.

B. Particle-size distributions and the dynamic sintering curves

The particle sizes and particle-size distributions of the synthesized powders were analyzed with a static light-scattering method, using a laser granulometer (Microtrac S3500 Particle Size Analyzer). Prior to the measurements, the powder samples were suspended in isopropanol and then placed in an ultra-sound bath (Iskra Sonis 4) for a few minutes in order to break up the agglomerates. The powders are described with the area particle size distribution, the cumulative curve, and with the 90% particle size limit (d_{90}), 50% particle size limit (d_{50}), and 10% particle size limit (d_{10}). The dynamic sintering curves of the powder compacts were recorded with a heating rate of 5 °C/min using an optical dilatometer (Leitz V. 1A, Leitz, Wetzlar).

The particle size distributions of the two powders shown in Figure S1a are narrow. The d_{90} of the Mech and Col are 0.93 μm and 0.56 μm, respectively. The bimodal distribution of the Mech powder indicates the presence of agglomerates.

(a)　　　　　　　　　　　　　　　　　　　　　(b)
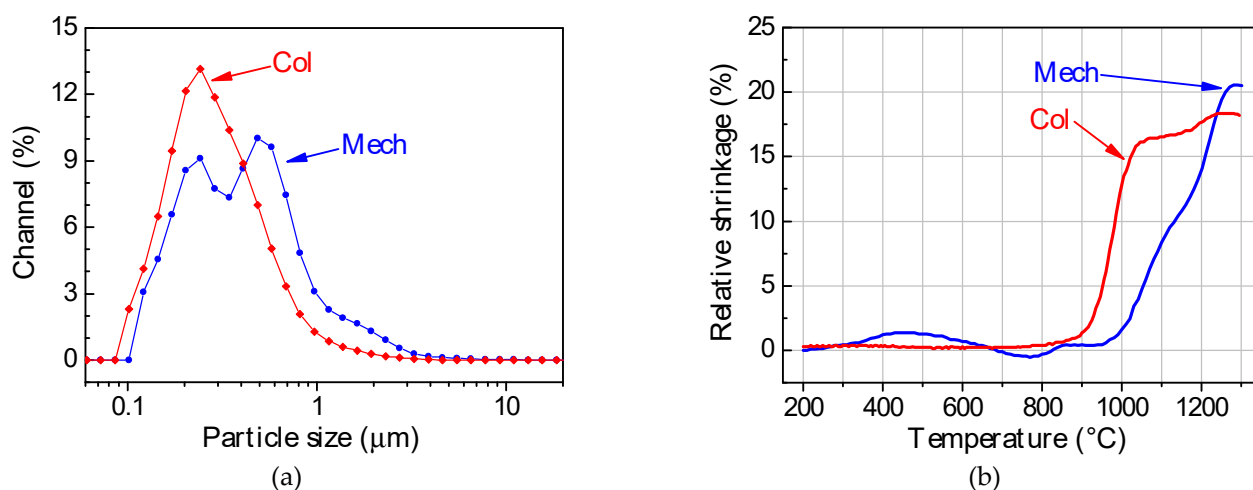
Figure S1. (**a**) Particle size distributions and (**b**) the dynamic sintering curves of the Col (red) and Mech (blue) powders. Lines are a guide for the eye. The dynamic sintering curves of both powder compacts reveal different shrinkage behaviors, see Figure S1b. Namely, the Col sample starts to shrink at a lower temperature than the Mech, ~900 °C as opposed to ~950 °C, but with a narrower shrinkage interval. Plateau of the maximum shrinkage was achieved at ~1050 °C and 1250 °C in the cases of the Col and Mech samples, respectively, suggesting sintering in the presence of a liquid phase in the Col sample in contrast to solid-state sintering in the Mech sample [8].

C. X-ray diffraction analysis

The powder was analyzed with an X-ray diffractometer (XRD; X'Pert PRO MPD, PANalytical, Almeo) using Cu-K$_{\alpha 1}$ radiation. The XRD patterns were recorded in the 2Θ range from 10° to 70° using a 1D detector (X'Celerator, PANalytical, Almeo) with a capture angle of 2.122°. The exposure time for each step was 100 s and the interval between the obtained data points was 0.034°.

The XRD patterns of the synthesized powders are collected in Figure S2. Although in both cases the perovskite PMN is a major phase, the full width at half maximum of the Col peaks is lower, indicating a larger crystallite size. The Mech powder, on the other hand, contains a large fraction of the amorphous phase. In the Col powder, peaks of pyrochlore phases are observed (Py, green in Figure S2) and traces of the PbTiO$_3$ phase (PT, violet in Figure S2). These phases further react to form the perovskite phase during the sintering stage (see Figure S3).
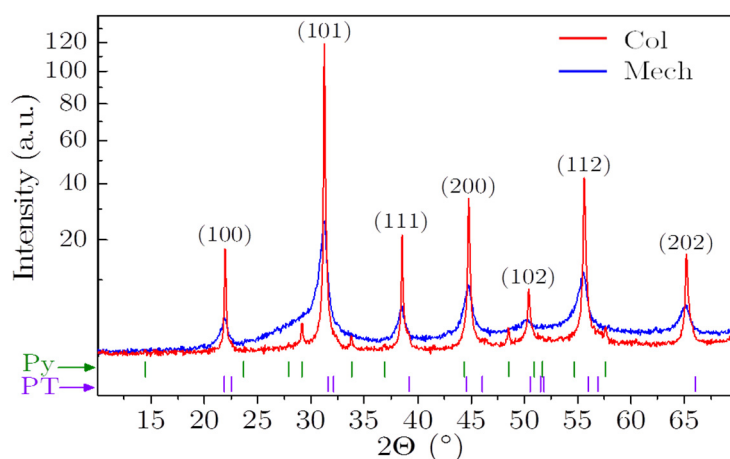

Figure S2. XRD patterns of the Col (red) and Mech (blue) powders. The peaks, denoted with Miller indices, correspond to the PMN (JCPDS 81-0861). Green and violet tick marks correspond to the peak positions of the cubic Pb$_{1.86}$Mg$_{0.24}$Nb$_{1.76}$O$_{6.5}$ (Py; JCPDS 82-0338) and tetragonal PT (JCPDS 078-0299), respectively. Note the square-root scale of the y-axis. The XRD patterns of the crushed Col and Mech ceramic pellets are collected in Figure S3. According to the XRD analysis, both samples consisted only of the perovskite pseudo-cubic phase (JCPDS 81-0861).
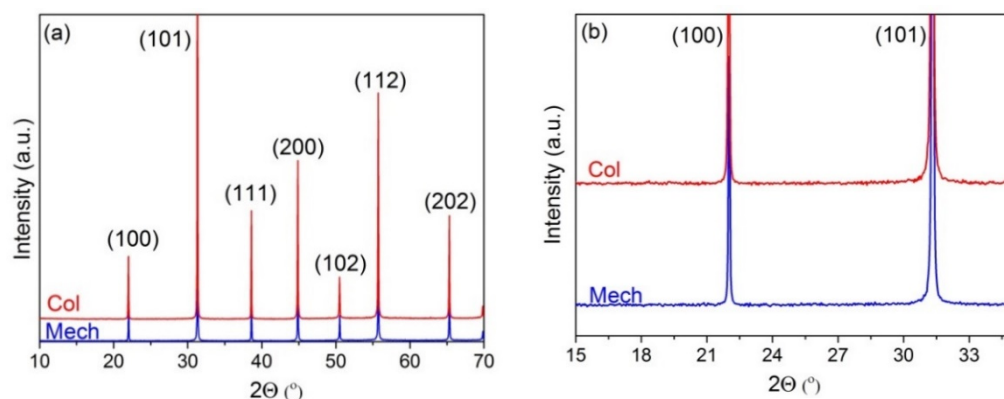
Figure S3. (**a**) XRD pattern of the sintered Col and Mech PMN-10PT ceramics. All the peaks correspond to the perovskite phase (JCPDS 81-0861). (**b**) An enlarged 2Θ region from 15 to 35°.

D. Wavelength-dispersive X-ray spectrometer analysis

Wavelength-dispersive X-ray spectrometer (WDXS) analysis performed in SEM (FE-SEM; JEOL JSM-7600) was used to determine the chemical composition of the sintered ceramics. The accelerating voltage was 20 kV. A <111> single crystal with the PMN-32PT composition was used as a reference sample (APC International, Ltd. Mackeyville, PA) for the quantification of the Pb, Ti, Nb, and Mg contents. The X-ray intensities for the Pb-Lα spectral line were measured with a LIF (lithium fluoride) crystal, the Ti-Kα, Nb-Lα, and Zr-Lα spectral lines were measured with a PET (pentaerythritol) crystal, and the Mg-Kα spectral line with a TAP (thallium acid phthalate) crystal. The oxygen was calculated from the stoichiometry. The obtained results, which are summarized in Table 1 of the main text, represent the average of about ten measurements.
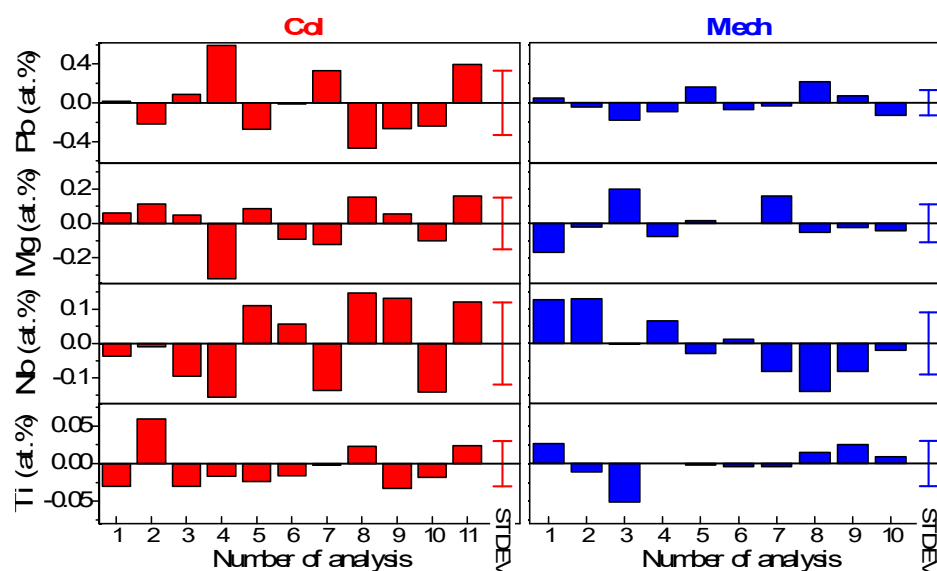
Figure S4. Deviation of the concentration for individual elements with regard to their nominal concentrations. The results are given together with STDEV for the Col and Mech ceramics. The analyses were performed on the grain interiors.

References

[1] Perantie J.; Tailor H. N.; Hagberg J.; Jantunen H.; Ye Z.-G.: Electrocaloric properties in relaxor ferroelectric (1-x)Pb(Mg$_{1/3}$Nb$_{2/3}$)O$_3$–xPbTiO$_3$ system. *J. Appl. Phys.* 2013, 114, 174105 1–6.

[2] Molin C.; Sanlialp M.; Shvartsman V. V.; Lupascu D. C.; Neumeister P.; Schoenecker A.; Gebhardt S.: Effect of dopants on the electrocaloric effect of 0.92Pb(Mg$_{1/3}$Nb$_{2/3}$)O$_3$–0.08PbTiO$_3$ ceramics. *J. Eur. Ceram. Soc.* 2015, 35, 2065–2071.

[3] Hagberg J.; Uusimaki A.; Jantunen H.: Electrocaloric characteristics in reactive sintered 0.87Pb(Mg$_{1/3}$Nb$_{2/3}$)O$_3$–0.13PbTiO$_3$. *Appl. Phys. Lett.* 2008, 92, 132909 1–3.

[4] Sebald G.; Seveyrat L.; Guyomar D.; Lebrun L.; Guiffard B.; Pruvost S.: Electrocaloric and pyroelectric properties of 0.75Pb(Mg$_{1/3}$Nb$_{2/3}$)O$_3$–0.25PbTiO$_3$ single crystals. *J. Appl. Phys.* 2006, 100, 124112 1–6.

[5] Rozic B.; Malic B.; Ursic H.; Holc J.; Kosec M.; Neese B.; Zhang Q. M.; Kutnjak Z.: Direct measurements of the giant electrocaloric effect in soft and solid ferroelectric materials. *Ferroelectrics* 2010, 405, 26–31.

[6] Vrabelj M.; Ursic H.; Kutnjak Z.; Rozic B.; Drnovsek S.; Bencan A.; Bobnar V.; Fulanovic L.; Malic B.: Large electrocaloric effect in grain-size-engineered 0.9Pb(Mg$_{1/3}$Nb$_{2/3}$)O$_3$–0.1PbTiO$_3$. *J. Eur. Ceram. Soc.* 2016, 36, 75–80.

[7] Ursic H.; Vrabelj M.; Fulanovic L.; Bradesko A.; Drnovsek S.; Malic B.: Specific heat capacity and thermal conductivity of the electrocaloric (1-x)Pb(Mg$_{1/3}$Nb$_{2/3}$)O$_3$–xPbTiO$_3$ ceramics between room temperature and 300°C. Informacije MIDEM, *Journal of Microelectronics, Electronic Components and Materials (open access)* 2015, 45, 260–265.

[8] Nielsen E.R.; Ringgaard E.; Kosec M.: Liquid-phase sintering of Pb(Zr,Ti)O$_3$ using PbO–WO$_3$ additive, *J. Eur. Ceram. Soc.* 2002, 22, 1847–1855.

[9] Ursic H.; Bencan A.; Drazic G.; Esteves G.; Jones J. L.; Usher T. M.; Rojac T.; Drnovsek S.; Deluca M.; Jouin J.; Bobnar V.; Trefalt G.; Holc J.; Malic B.: Unusual structural-disorder stability of mechanochemically derived-Pb(Sc$_{0.5}$Nb$_{0.5}$)O$_3$. *J. Mater. Chem. C* 2015, 3, 10309–10315.

[10] Rojac T.; Benčan A.; Ursic H.; Malic B.; Kosec M.: Synthesis of a Li-and Ta-modified (K,Na)NbO$_3$ Solid solution by mechanochemical activation. *J. Am. Ceram. Soc.* 2008, 91, 3789–3791.